iScience

CellPress
OPEN ACCESS

Article

Plasma and urine proteomics and gut microbiota analysis reveal potential factors affecting COVID-19 vaccination response

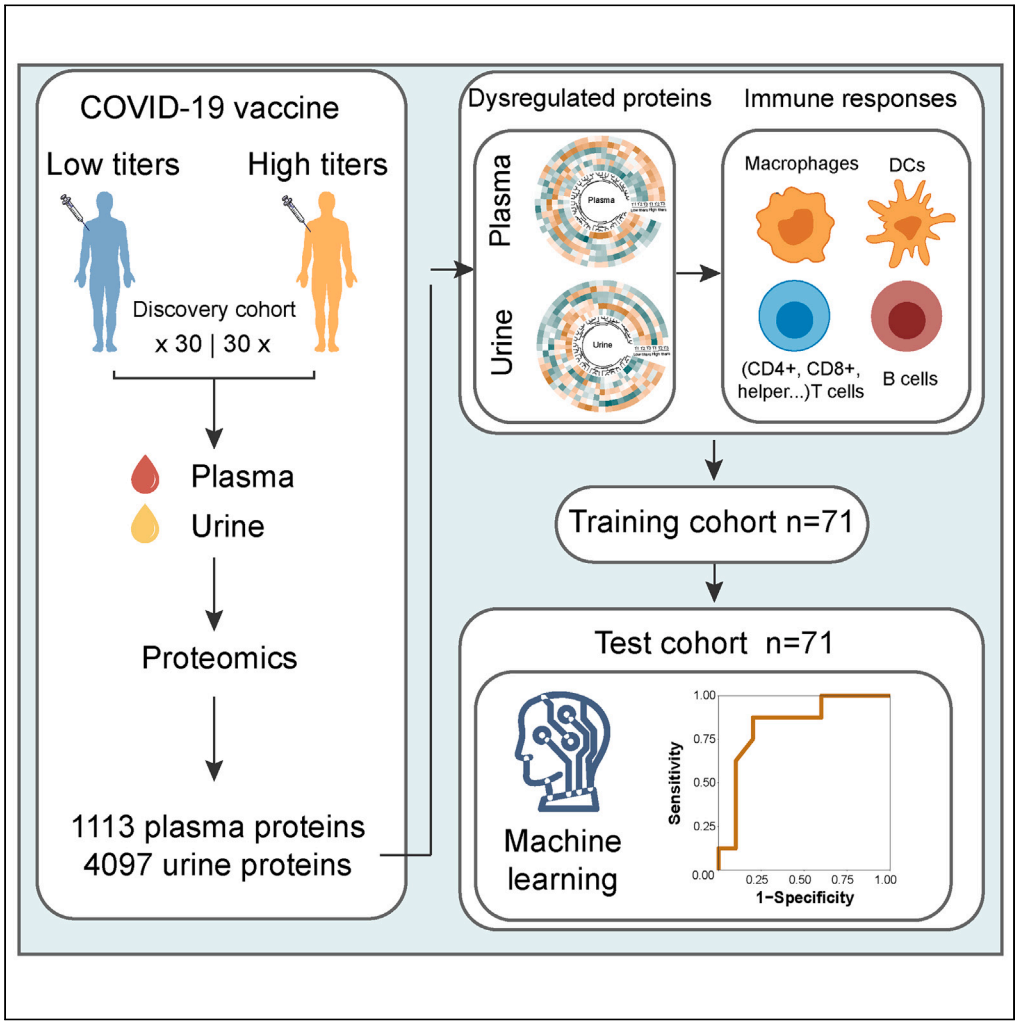

Changjiang Hu, Weichao Hu, Bo Tang, ..., Zhongjun Li, Tiannan Guo, Shiming Yang

dongzhen@westlake.edu.cn (Z.D.)
johnneyusc@gmail.com (Z.L.)
guotiannan@westlake.edu.cn (T.G.)
yangshiming@tmmu.edu.cn (S.Y.)

Highlights

Plasma LXR/FXR activation is associated with ACE2-RBD-inhibiting antibody titer

Urine proteins correlate with neutralizing antibodies production

Gut microbiota is related with plasma and urine proteins, and vaccination response

Integration of plasma, urine data, and clinical features predicts vaccination response

Hu et al., iScience 27, 108851
February 16, 2024
https://doi.org/10.1016/j.isci.2024.108851

iScience

CellPress
OPEN ACCESS

Article

Plasma and urine proteomics and gut microbiota analysis reveal potential factors affecting COVID-19 vaccination response

Changjiang Hu,[1,2,3,4,5,7] Weichao Hu,[1,2,3,4,5,7] Bo Tang,[1,7] Qiyu Bao,[1,7] Xingyu Jiang,[6,7] Li Tang,[1] He Wang,[2,3,4,5] Lijiao He,[1] Moyang Lv,[1] Yufeng Xiao,[1] Cheng Liu,[1] Xinzhe Li,[1] Yunyi Liu,[1] Jie Li,[1] Guiping Huang,[1] Zhen Dong,[2,3,4,5,*] Zhongjun Li,[6,*] Tiannan Guo,[2,3,4,5,*] and Shiming Yang[1,8,*]

SUMMARY

The efficacy of COVID-19 vaccination relies on the induction of neutralizing antibodies, which can vary among vaccine recipients. In this study, we investigated the potential factors affecting the neutralizing antibody response by combining plasma and urine proteomics and gut microbiota analysis. We found that activation of the LXR/FXR pathway in plasma was associated with the production of ACE2-RBD-inhibiting antibodies, while urine proteins related to complement system, acute phase response signaling, LXR/FXR, and STAT3 pathways were correlated with neutralizing antibody production. Moreover, we observed a correlation between the gut microbiota and plasma and urine proteins, as well as the vaccination response. Based on the above data, we built a predictive model for vaccination response (AUC = 0.85). Our study provides insights into characteristic plasma and urine proteins and gut microbiota associated with the ACE2-RBD-inhibiting antibodies, which could benefit our understanding of the host response to COVID-19 vaccination.

INTRODUCTION

The coronavirus disease 19 (COVID-19) pandemic has caused unprecedented morbidity and mortality globally,[1–3] underscoring the urgent need for effective vaccines.[4,5] To date, hundreds of COVID-19 vaccine candidates have been developed, and over 100 have progressed to clinical trials.[6,7] These vaccines, including mRNA vaccines, viral vector vaccines, protein subunit vaccines, and inactivated viral vaccines, have demonstrated potent antibody responses in humans and have undergone extensive clinical evaluation.[8] Nevertheless, the immune response to vaccination varies greatly among individuals, highlighting the need to identify molecular predictors based on individual baseline conditions and to elucidate their biological basis.

CoronaVac immunization leads to activation of humoral and complement responses.[9] Additionally, this vaccine has been found to modulate the TCA cycle and amino acid metabolism.[9] Notably, neutralizing antibodies are detected earlier in female individuals compared to males, and the peak neutralizing antibody titers are inversely correlated with age and BMI.[9] The cytokine/chemokine signatures IL-15, IFN-γ, and IP-10/CXCL10 have been associated with effective immune responses to SARS-CoV-2 in BNT162B2 mRNA vaccine recipients. Nevertheless, further systematic investigations are required to fully understand the immune response to COVID-19 vaccination.

Previous studies have suggested that baseline immune status prior to vaccination may predict the outcomes of other vaccines, such as those against influenza virus, yellow fever virus, hepatitis B virus, and malaria.[10] For instance, peripheral blood mononuclear cell (PBMC) subpopulation frequencies predicted the immune response to influenza vaccination independently of age and preexisting antibody titers,[11] while inflammatory response transcripts and proinflammatory innate immune cells were associated with the response to HBV vaccination.[12] White blood cell (WBC) count was also found to be a predictive biomarker for the response to malaria vaccination.[13] Additionally, several proteins expressed in plasma and urine have been linked to the severity of COVID-19.[14–16]

Given this evidence, we propose a possible correlation between plasma and urine proteomics and the efficacy of COVID-19 vaccination. To identify biomarkers associated with COVID-19 vaccination, we studied the proteomic profiles of plasma and urine collected at baseline

[1]Department of Gastroenterology, Xinqiao Hospital, Third Military Medical University, Chongqing 400037, China
[2]iMarkerlab, Westlake Laboratory of Life Sciences and Biomedicine, Key Laboratory of Structural Biology of Zhejiang Province, School of Life Sciences, Westlake University, Hangzhou, Zhejiang Province, China
[3]Institute of Basic Medical Sciences, Westlake Institute for Advanced Study, Hangzhou, Zhejiang Province, China
[4]Research Center for Industries of the Future, Westlake University, 600 Dunyu Road, Hangzhou 310030, Zhejiang, China
[5]Center for Infectious Disease Research, Westlake University, 18 Shilongshan Road, Hangzhou 310024, Zhejiang, China
[6]Laboratory Medicine Center, Xinqiao Hospital, Third Military Medical University, Chongqing 400037, China
[7]These authors contributed equally
[8]Lead contact
*Correspondence: dongzhen@westlake.edu.cn (Z.D.), johnneyusc@gmail.com (Z.L.), guotiannan@westlake.edu.cn (T.G.), yangshiming@tmmu.edu.cn (S.Y.)
https://doi.org/10.1016/j.isci.2024.108851

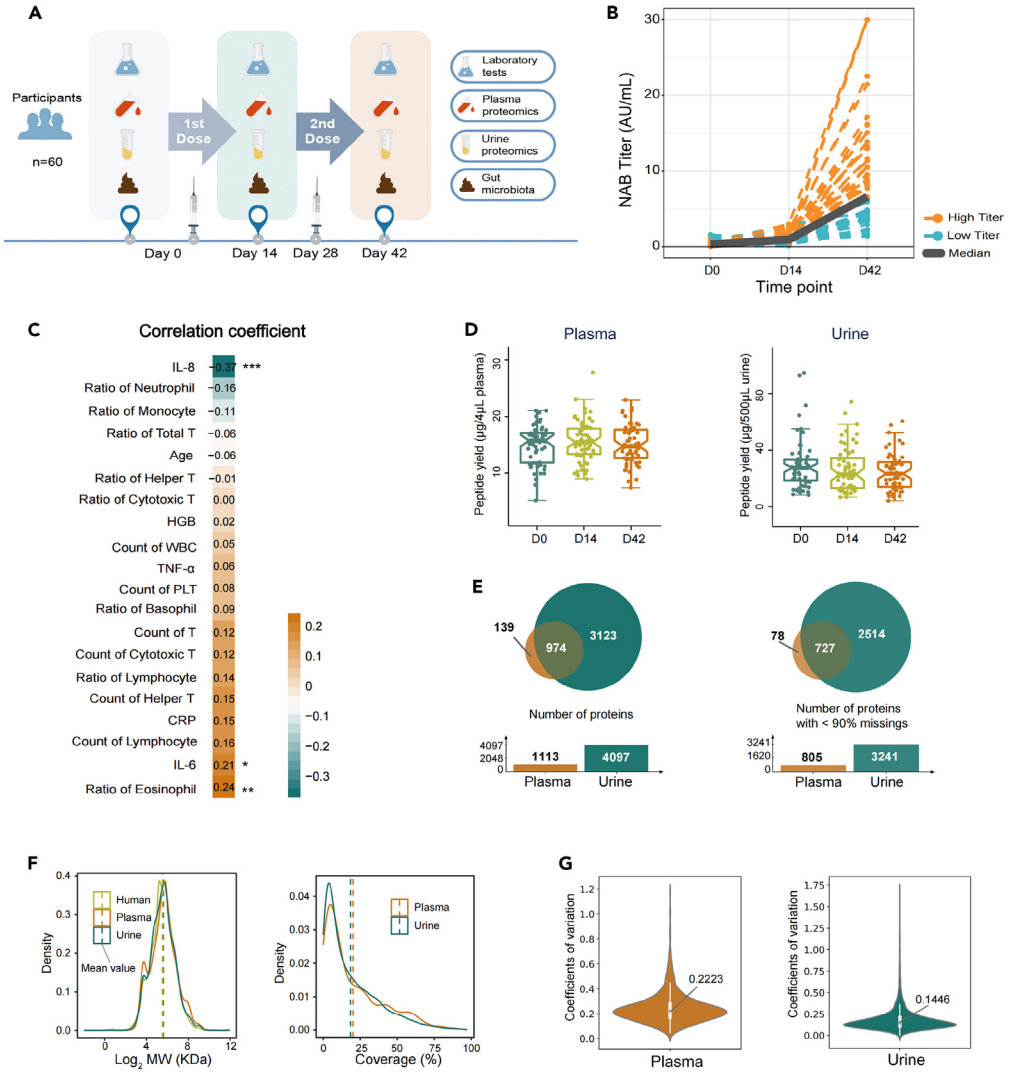

Figure 1. Healthy subjects received inactivated vaccines against COVID-19

(A) Workflow for the enrollment of healthy subjects and sample collection.

(B) The ACE2-RBD-inhibiting antibody changes of the 60 participants after the two doses of vaccination at D0, D14 and D42. According to the median neutralizing antibody levels at Day 42 (6.6 AU/mL), they were equally split into two groups, top 50 percent as higher titers and bottom 50 percent as low responders.

(C) Pearson correlation coefficients between the change in clinical laboratory indicators and ACE2-RBD-inhibiting antibody levels during Day 0 and Day 42 were calculated. The amber represents a positive correlation, while the turquoise represents a negative correlation (n = 60).

(D) The peptide yield from 4 μL plasma and 500 μL urine at D0, D14, and D42.

(E) The protein number of plasma and urine and the protein with <90% missing values.

(F) The molecular weight (MW) and sequence coverage distributions of quantified protein in plasma, urine, and the entire human proteome.

(G) The median CV of the plasma and urine proteomics data.

(D0), 14 days after the first dose (D14), and another 14 days after the second dose (D42) from three independent cohorts. Our aim is to reveal the association between ACE2-RBD inhibiting antibody development and baseline plasma and urine proteomics, as well as clinical characteristics.

RESULTS

Clinical features of the healthy BBIBP-CorV vaccine recipients correlated with ACE2-RBD-inhibiting antibody production

We enrolled a total of 60 healthy individuals who received two doses of the BBIBP-CorV vaccine, and no apparent adverse events were observed. To investigate the relationship between clinical features and the development of ACE2-RBD-inhibiting antibodies, we collected longitudinal plasma and urine samples at three time points (D0, D14, and D42) for laboratory tests and proteomic analysis (Figure 1A). Prior

to vaccination, all individuals tested negative for ACE2-RBD-inhibiting antibodies, and 93% of the vaccine recipients seroconverted at 42 days. As shown in Figure 1B, the antibody concentration markedly increased on Day 14 and Day 42. Most laboratory tests showed no significant changes at Day 42, including C-reactive protein (CRP), WBC count, ratio of neutrophil, ratio of lymphocyte, ratio of monocyte, ratio of eosinophils, ratio of basophil, hemoglobin (HGB), PLT count, ratio of helper T, ratio of cytotoxic T cell, lymphocyte count, total T cell count, helper T cell count, cytotoxic T cell count, and TNF-α. However, IL-6, an important proinflammatory cytokine produced by antigen-presenting cells, significantly increased after vaccination (Table S1). It has been reported that IL-6 plays a crucial role in the acquired immune response by stimulating antibody production and effector T cell development. Moreover, Pearson correlation coefficients between the change in clinical laboratory indicators and ACE2-RBD-inhibiting antibody levels during Day 0 and Day 42 were calculated. We found the ratio of eosinophil and IL-6 levels were significantly positively correlated with the vaccination response with correlation coefficients of 0.24 and 0.21, while IL-8 was negatively correlated with the vaccination response with correlation coefficient of −0.37 (Figure 1C). In order to compare the high and low responders, we artificially defined neutralizing antibodies level above 50th percentile of the cohort as high titers (higher than the median level 6.6 AU/mL, n = 30), while those below 50th percentile as low titers (lower than 6.6 AU/mL, n = 30). We analyzed the difference of clinical laboratory indicators between these two groups by using the Wilcoxon's rank-sum test (two-sided). At Day 0, age and count of helper T cells of high-degree response group were significantly lower than low-degree response group (Table S2). At Day 42, count of lymphocytes, total T cells, and helper T cells were significantly higher than low-degree response group (Table S3).

Dynamics of proteomics profiling of plasma and urine after vaccination

We used a tandem mass tag (TMT)-based proteomics approach to analyze the 180 plasma and 180 urine samples collected on Day 0, Day 14, and Day 42 from the 60 healthy volunteers. PCA showed no significant batch effect between different batches of the plasma and urine proteins (Figures S1A and S1B). The peptide yields from plasma and urine showed no significant differences among the three different time points, indicating the stability of the sample preparation (Figure 1D). Altogether, 1113 and 4097 proteins were identified and quantified in plasma and urine, respectively. After filtering out proteins with over 90% missingness, we focused on 805 blood proteins and 3241 urine proteins (Figure 1E). The molecular weight (MW) distributions of plasma and urine were comparable to those in the human proteome, consistent with previous reports.[17,18] The urine proteome contained more proteins with relatively low sequence coverage (Figure 1F). In the quality control analysis, the median coefficients of the variation values for the plasma and urine were 22.23% and 14.46%, respectively (Figure 1G). These analyses suggest that the thus acquired proteome data are of high technical quality.

The subcellular localization of proteins was subsequently analyzed. Figure S2A shows that secreted proteins constituted 40% of the plasma proteins, followed by cytoplasmic and membrane proteins, while the cytoplasmic proteins (24%) and secreted proteins (20%) were the most abundant in urine. In the overlap of the two groups, the secreted proteins constituted 45%. GO analysis showed that immune response, complement activation, and coagulation were enriched in the secreted proteins of both plasma and urine (Figure S2B). In addition, most enriched pathways, such as actin filament organization and actin filament polymerization, were quite similar in the cytoplasmic proteins derived from plasma and urine (Figure S2C).

The plasma and urine protein changes after vaccination were then analyzed. REAC and KEGG analysis showed that the DEPs in plasma after vaccination were related to Glycolysis, Cellular response to chemical stress, TCA cycle, Detoxification of reactive oxygen species (Figure 2A). Figure 2B revealed that DEPs in plasma annotated by Uniprot database were associated with glycolysis, immunocyte migration, and immunoregulation. Interestingly, the mannose receptor, C type 1 (MRC1), an endocytic receptor expressed by populations of dendritic cells and macrophages, was significantly increased after vaccination (Figure 2C). MRC1 functions include a role in antigen cross-presentation, clearance of endogenous proteins, pathogen detection.[19] Furthermore, pro-platelet basic protein (PPBP), a potent chemoattractant and activator of neutrophils, was also increased at D42. Neutrophils are traditionally recruited to sites of inflammation in response to infectious and inflammatory stimuli. A recent study revealed that they could indirectly influence antigen presentation by interacting with DCs or directly expressing major histocompatibility complex (MHC).[20]

REAC and KEGG analysis revealed the DEPs in urine were related to hemidesmosome assembly and apoptotic cleavage of cellular proteins (Figure 2D). Urine DEPs annotated by Uniprot were associated with immunocyte chemotaxis, glycolysis, and immunoregulation (Figure 2E). Notably, Arginase 1 (ARG1) plays a vital role in L-arginine homeostasis, which is a critical regulator of innate and adaptive immune responses, resulting in suppressed T cell and natural killer (NK) cell proliferation and cytokine secretion. In addition, Figure 2F illustrates that ARG1 was significantly elevated after two vaccination doses. The dynamic changes in the proteomics profiles of plasma and urine following vaccination suggest an altered acquired immune response to COVID-19 vaccination.

The differences in plasma proteomics profiles between high and low responders

To further characterize the underlying molecular mechanisms responsible for different immune responses to the BBIBP-CorV vaccine, we compared the plasma and urine proteomics profiles between high and low responders. There were 67, 52, and 55 dysregulated proteins in plasma at D0, D14, and D42, respectively (Table S4). At D0, the differentially expressed proteins were associated with complement and coagulation cascades and platelet degranulation (Figure 3A), which is consistent with the immune response induced by COVID-19 infection.[15] Additionally, IPA analysis showed that the pathways at different time points were enriched in coronavirus disease, glucocorticoid receptor signaling, liver X receptor (LXR)/retinoid X receptor (RXR), and farnesoid X receptor (FXR) (Figure 3B). Notably, kininogen-1 (KNG1) was found to be decreased in the high respond group at D0. KNG1 is the precursor protein of the kallikrein-kinin system (KKS), which includes high molecular weight (HMW) and low molecular weight (LMW) KNGs. HMW KNG interacts with plasma kallikrein to produce bradykinin (BK), a

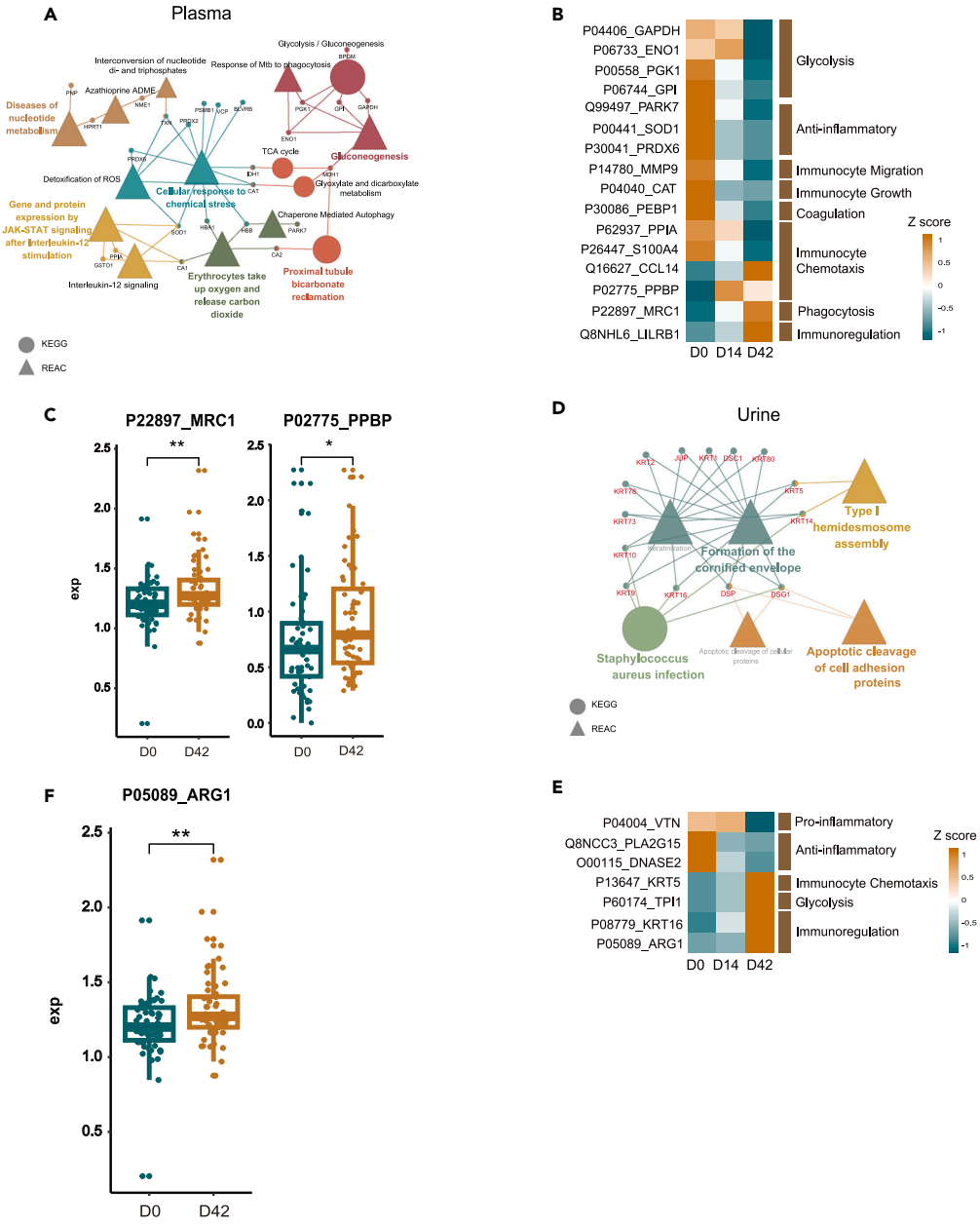

Figure 2. Dynamics of proteomics profiling of plasma and urine after vaccination

(A) REAC and KEGG pathway enrichment analysis of the differentially expressed proteins (DEPs) in plasma after vaccination visualized by ClueGO plugin of Cytoscape. The DEPs between D0 and D42 (n = 60) were analyzed by Wilcoxon test ($p < 0.05$).

(B) Heatmap of plasma DEPs involved in immune response at D0, D14 and D42 (n = 60).

(C) MRC1 and PPBP expression in plasma at D0 and D42, *p* value was calculated by Wilcoxon test ($p < 0.05$).

(D) REAC and KEGG analysis of the DEPs in urine after vaccination visualized by ClueGO plugin of Cytoscape. The DEPs between D0 and D42 (n = 60) were analyzed by Wilcoxon test ($p < 0.05$).

(E) Heatmap of urine DEPs involved in immune response at D0, D14 and D42 (n = 60).

(F) ARG1 expression in plasma at D0 and D42, *p* value was calculated by Wilcoxon test ($p < 0.05$).

substance that has been shown to suppress MHC Class I upregulation and proinflammatory cytokine production, and to inhibit the IFN-induced phosphorylation of STAT2 molecules and subsequent induction of IFN-responsive genes.[21] Apolipoprotein L1 (APOL1) and Complement C3 (C3) proteins, both of which are involved in the LXR/FXR pathway, increased in the high response group (Figure 3C). LXR activation depletes Myeloid-derived suppressor cells (MDSCs) and elicits T cell activation.[22] Moreover, LXR agonists have been shown to augment anti-tumor responses when combined with checkpoint inhibitors or adoptive T cell therapies.[22] Our group has previously reported that LXR/RXR

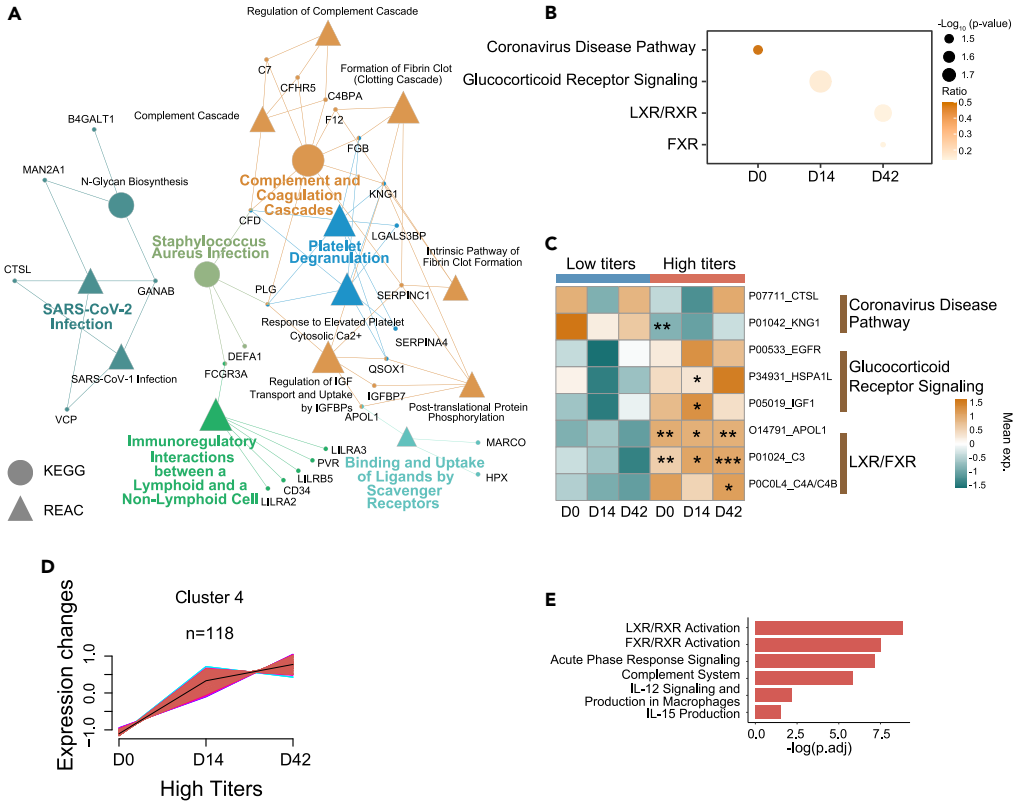

Figure 3. Differences of plasma proteomics profiles between high and low responders

(A) REAC and KEGG analyses of plasma DEPs enriched pathways between high (n = 30) and low responders (n = 30) at D0 visualized by ClueGO plugin of Cytoscape. The R package limma was used to analyze DEPs (BH adjusted $p < 0.05$).

(B) IPA analysis of the plasma DEPs enriched pathways between high (n = 30) and low responders (n = 30) at D0, D14 and D42.

(C) Heatmap of the IPA enrichment analysis of plasma DEPs at the indicated time points (Wilcoxon test, $p < 0.05$).

(D) Mfuzz analysis of dynamic changes of plasma proteins in the high-response group (Cluster 4, n = 118).

(E) GO gene enrichment of the plasma DEPs from Cluster 4.

inhibition contributed to prolonged RNA shedding in COVID-19, indicating that the LXR/RXR pathway is not only correlated with the RNA shedding period but also associated with the vaccination response to COVID-19.[23] The bile acid sensor FXR, expressed in cells related to innate immunity, including macrophages, liver resident macrophages, the Kupffer cells, natural killer cells, and dendritic cells, was required for immune-regulatory activities.[24] FXR agonism attenuates inflammation-driven immune dysfunction, making the immunomodulatory effects of FXR clinically relevant.[24] Finally, we divided the dysregulated plasma proteins in both high and low responders into eight groups based on their dynamics using Mfuzz (Figures S3A and S3B). The cluster 4 of the high response group showed a similar increasing trend with the neutralizing antibody (Figure 3D), while both LXR and FXR activation were significantly enriched in this cluster (Figure 3E). Collectively, these findings suggest a more substantial adaptive immune process in the high-respond group with activation of LXR/FXR.

Regulated urinary proteins between high and low responders

We conducted a comparison of urine proteomic profiles between high and low responders and found 97, 184, and 157 dysregulated proteins at D0, D14, and D42, respectively (Table S5). Prior to vaccination, the differentially expressed proteins were linked to detoxification of reactive oxygen species and interleukin-10 signaling (Figure 4A). Additionally, IPA analysis revealed that Th1 and Th2 activation were most significantly enriched at Day 0, while phagosome maturation was enriched at Day 14, and granulocyte adhesion and diapedesis were enriched at Day 42 (Figure 4B). Interestingly, the protein expression pattern demonstrated that the majority of proteins involved in the aforementioned pathways were expressed at higher levels during the entire vaccination period in the high response group (Figure 4C). Furthermore, we clustered the dysregulated urine proteins in both high and low responders into eight groups using Mfuzz (222C and S3D). Cluster 6 of the high response group displayed a consistent ascending pattern similar to that of Neutralizing antibody (NAB) production (Figure 4D). For this cluster, the complement system, acute phase response signaling, LXR/RXR, FXR/RXR, and STAT3 pathways were enriched, which were quite similar to those identified in plasma (Figure 4E). Previous studies have demonstrated that aberrant regulation of physiological processes, including the complement system, macrophage functions, and platelet degranulation, was observed in the plasma of severe cases of

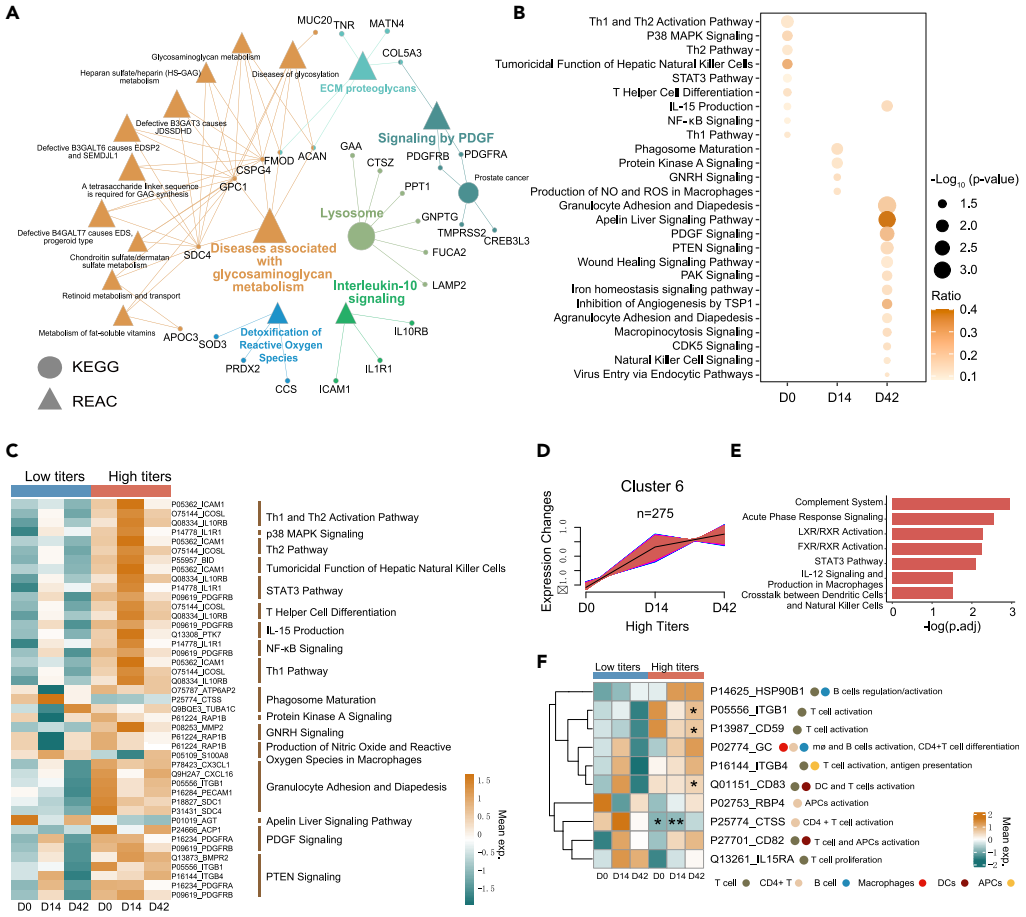

Figure 4. Difference of urine proteomics profiling between high and low responders

(A) REAC and KEGG analyses of urine DEPs enriched pathways between high (n = 30) and low responders (n = 30) at D0 visualized by ClueGO plugin of Cytoscape. The R package limma was used to analyze DEPs (BH adjusted p < 0.05).

(B) IPA analysis of the urine DEPs enriched pathways between high (n = 30) and low responders (n = 30) at D0, D14 and D42.

(C) Heatmap of the IPA enrichment analysis of urine DEPs at the indicated time points.

(D) Mfuzz analysis of dynamic changes of urine proteins in the high-response group (Cluster 6, n = 275).

(E) GO gene enrichment of the urine DEPs from Cluster 6.

(F) Heatmap of the urine proteins involved in the vaccination production process. The DEPs between high and low responders were compared at different time points, and *p* values (D0, D14 and D42) were calculated by the Wilcoxon test ($p < 0.05$).

COVID-19.[15,25] Immune-related pathways, including coagulation system, acute phase response signaling, and LXR/RXR activation, were up-regulated in both plasma and urine of COVID-19 patients, and the STAT3 pathway was enriched in the plasma proteins from COVID-19 patients.[14] Coagulation dysfunction was a potential risk factor for adverse outcomes in COVID-19.[26] STAT-3 can also participate in the induction of inflammatory responses during coronavirus infections and thus contribute to the pathogenesis of COVID-19.[27] Moreover, most of the proteins involved in the vaccination response process, including the activation of T and B cells, proliferation, and differentiation of T cells, were expressed at higher levels during the entire vaccination period in the high response group (Figure 4F). These findings suggest that immune responses from urine proteome may correlate with the postvaccination titers of neutralizing antibodies.

Differential expression of cytokines and their receptors between high and low responders

Uncontrolled inflammation is a major contributor to the high mortality rate observed in COVID-19 patients.[28] In our study, we investigated the expression of cytokines and their receptors in plasma and urine samples collected from high and low responders. We identified a total of 59 cytokines and their receptors in plasma and 218 in urine, which were classified into six types, namely interleukins, interferon, the transforming growth factor-b (TGF-β) family, tumor necrosis factor (TNF) family, chemokines and other cytokines (Figure S4A). We further analyzed the expression of these cytokines in relation to different immune cells, and identified seven cytokines and receptors that were significantly dysregulated in different time points between high and low response groups in the plasma, and thirty-nine in the urine (Figure 5A; Table S6). Among them, Alpha-defensin 1 (DEFA1) was significantly increased in the plasma of the high response group before vaccination (Figure 5A).

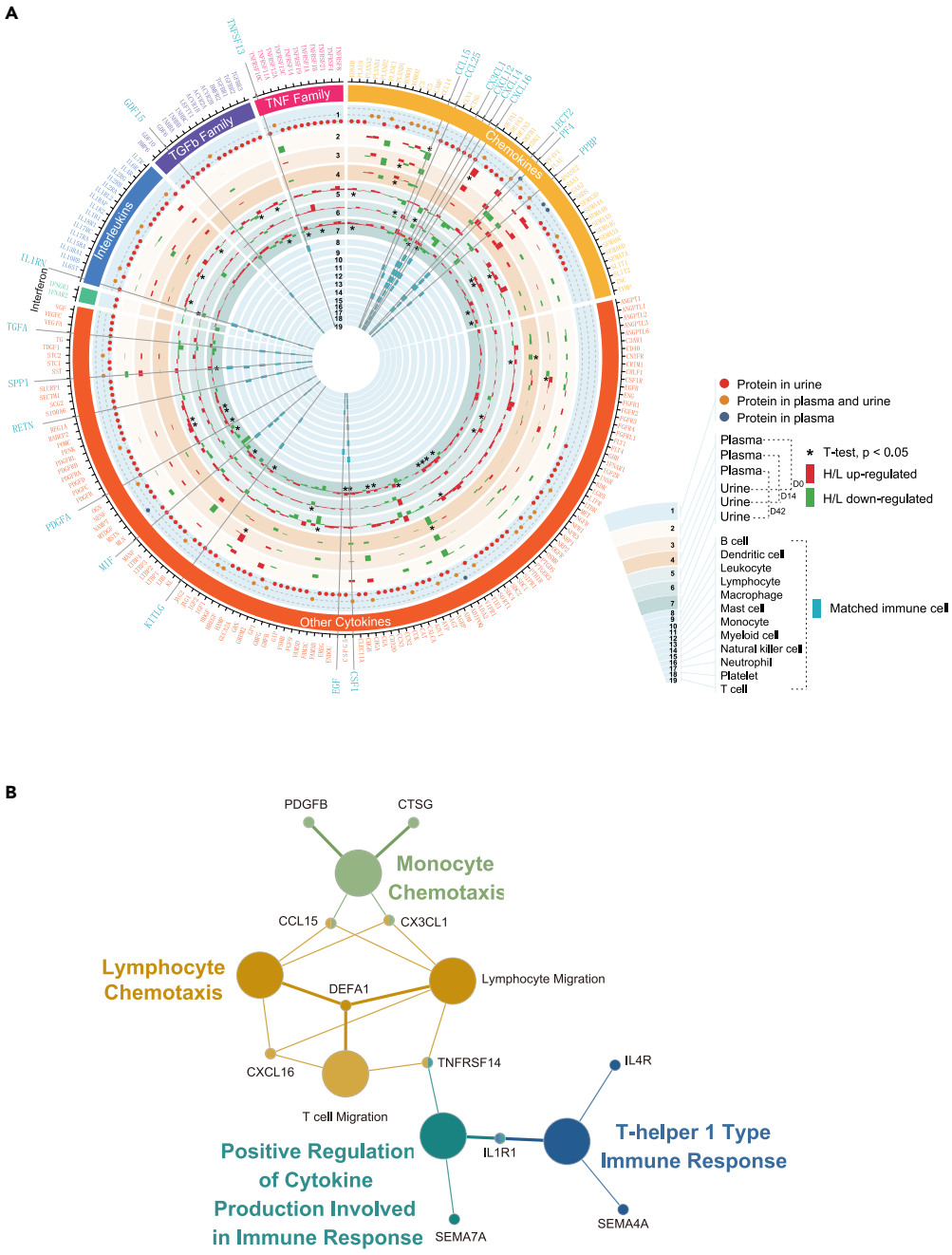

Figure 5. Differences of cytokines and their receptors between high and low responders

(A) Differentially expressed plasma and urine cytokines and their receptors between high and low responders at D0, D14 and D42. They were grouped into six groups, interleukins, transforming growth factor-b (TGF-β) family, tumor necrosis factor (TNF) family, interferon, chemokines, and other cytokines. *p* values were calculated by Wilcoxon test ($p < 0.05$). Twenty of them matched the different immune cells.

(B) GO enrichment of the above dysregulated cytokines and receptors between high and low responders visualized by ClueGO plugin of Cytoscape.

DEFA1 is an anti-microbial peptide of the innate immune system that is involved in phagocyte-mediated host defense, and its serum levels have been associated with disease severity in COVID-19 patients.[29,30] Figure 5A also shows that C-C Motif Chemokine Ligand 15 (CCL15) is dramatically decreased in the plasma of high response group. CCL15 could recruit suppressive monocytes to facilitate immune escape and disease progression in hepatocellular carcinoma.[31] In urine samples, most of the differentially expressed cytokines, including PLAUR, SDC4, PDGFRA, PDGFRB, SEMA4B, CRIM1, FAM3D, IL10RB, IL1R1, ACVR1B, and TGFBR1, were increased in the high response group. These modulated cytokines and receptors obtained from plasma and urine were enriched for lymphocyte chemotaxis and positive regulation of

cytokine production involved in immune response (Figure 5B). Moreover, fifty-four cytokines existing in both plasma and urine are shown at indicated time points (Figures S4B and S4C). Most of the cytokines shows different expression pattern in plasma and urine, which may be due to the different glomerular filtration and tubule reabsorption as reported previously.[14] Cytokines can activate innate immunity and then determine the responses of cells to adaptive immunity.[32] Cytokines can also modulate adaptive immunity. Various cytokines are elevated in COVID-19 patients, which may result in a cytokine storm in severe cases.[33] Our data suggest that the cytokines may be correlated with the production of the ACE2-RBD-inhibiting antibody.

A protein-based predictive model for vaccination responses

To predict the production of ACE2-RBD-inhibiting antibodies to SARS-CoV-2 before vaccination, a protein-based machine-learning model was developed by integrating clinical features and proteomic data collected on Day 0 (see the STAR Methods section). The study utilized a discovery cohort of 60 participants with both plasma and urine proteomic data, and two additional cohorts: a training cohort of 71 participants and a test cohort of 71 participants. Antibody titers above the 50th percentile of each cohort were considered high, while those below the 50th percentile were considered low. There was no significant difference in ACE2-RBD-inhibiting antibody titers among the discovery cohort (6.601 (4.126, 11.405)), training cohort (6.427 (4.636, 12.889)) and test cohort (6.427 (5.159, 13.290)). The clinical features of the above three cohorts at D0 were listed in Table S7. To further screen the features of plasma and urine protein for MRM analysis, the differentially expressed proteins of plasma and urine at D0, D14, and D42 were obtained (Figure 6A). After analyzing transitions of unique peptides of the DEPs generated by Skyline, 43 plasma and 62 urine proteins were selected as the input of the training model (listed in Table S8). Based on their expression robustness and the importance prioritized by random forest analysis, ten plasma proteins, including SERPINA1, KRT1, F10, KRT9, KLKB1, FGB, SERPINC1, LYVE1, AGT, and ICAM1, were selected to construct a 10-molecule model. The area under curve (AUC) value for the test cohort was 0.74 (Figure 6B). Similarly, ten urine proteins, including IGHG4, AGT, GP6, ALPL, F10, C7, CTSG, CD81, AQP1, and GLO1, were selected for the construction of another 10-molecule model. The AUC value is 0.67 (Figure 6C). The selected transition groups for the quantification of each peptide of the above proteins were listed in Figure S5. Moreover, eight clinical features, such as ratio of help T cell, lymphocyte count, IL-8, T cell count, TNF-α, age, ratio of monocyte, and IL-6, were selected to build an 8-feature model, and the AUC value was 0.68 (Figure 6D). Moreover, the AUC increased to 0.84 or 0.77 when the plasma or urine proteomics data were integrated with the clinical features, respectively (Figures 6E and 6F). Notably, after combining the above three indices, the above ten plasma proteins, ten urine proteins, and eight clinical features were used to build a 28-feature model with an AUC value of 0.85 (Figure 6G). To further validate our random forest model, we conducted 5-fold cross validation on our MRM datasets, the AUC values of the plasma, urine and clinical features were 0.74, 0.69, and 0.72, respectively (Figures S6A–S6C). The AUC increased to 0.77 or 0.75 when the plasma or urine proteomics data were integrated with the clinical features (Figures S6D and S6E). Moreover, after combining the above three indices, the AUC value reached 0.80 (Figure S6F). Overall, this study provides a protein-based machine-learning model that can predict the production of ACE2-RBD-inhibiting antibodies to SARS-CoV-2 before vaccination, which may be useful for identifying individuals who may not respond well to vaccination. The model incorporates clinical features and proteomic data, and the integration of these factors results in improved predictive performance.

The gut microbiome correlates with the ACE2-RBD inhibiting antibody

The gut microbiome is a key factor influencing the immune response to vaccination, and profiling the gut microbiota can provide insights into factors that impact robust and long-lasting immunity.[34,35] We profiled the characteristics of gut microbiota in the high response and low response group by metagenomic sequencing. For beta diversity, we used principal coordinate analysis (PCoA) based on the Bray–Curtis distance and observed significant clustering of gut microbiota between these two groups (ANOSIM, $p = 0.025$, Figure S7A). The Bray–Curtis distance rank between the high and low titer group was significantly different (ANOSIM, $p = 0.025$, Figure S7B). The high response group were primarily characterized by a predominance of *Enterococcus faecium*, *Prevotella bivia*, *Actinomyces massiliensis*, *Veillonella dispar*, *Veillonella_sp_T11011_6*, *Eubacterium_sp_CAG_38*, *Ruminococcus torques*, *Actinomyces odontolyticus*, while *Alistipes putredinis*, *Allisonella histaminiformans*, *Bacteroides clarus*, *Clostridium lavalense*, *Clostridium asparagiforme*, *Bacteroides eggerthii*, *Coprobacter fastidiosus*, *Sutterella parvirubra*, and *Blautia coccoides* are more abundant in the low response group (Figure S7C). The composition of microbial pathways further revealed different MetaCyc pathway between the above two groups. Compared to the low response group, petroselinate biosynthesis pathway was enriched in the high response group (Figure S7D). We next analyzed the correlation between the differential species at D0 and ACE2-RBD-inhibiting antibodies titers at D42. Figures 7A and S7E revealed that *V. dispar*, *A. histaminiformans*, *B. coccoides*, *A. putredinis*, and *C. lavalense* were correlated with the vaccination response (Spearman correlation, $p < 0.05$, $^{**}p < 0.01$). Furthermore, we further explored the correlation between the above five bacterial species and the plasma and urine protein at D0, respectively. The plasma proteins correlated with the bacterial abundance were listed in Figure 7B. KEGG and REAC revealed that the proteins correlated with *A. putredinis* abundance mainly involved in Glycolysis, JAK-STAT signaling and Interleukin-12 family signaling (Figure 7C). The urine proteins correlated with the five bacterial abundance were plotted in Figure 7D. KEGG and REAC revealed that the proteins correlated with *B. coccoides* abundance were involved in Coronavirus disease and selective autophagy (Figure 7E).

Our data provides insights into the molecular changes affecting the production of ACE2-RBD-inhibiting antibodies after COVID-19 vaccination, indicating potential plasma and urine markers for the improvement of vaccine response (summarized in Figure S8). Specifically, our analysis indicates that the differentially expressed proteins associated with the ACE2-RBD-inhibiting STAR antibody production were involved in the antigen recognition and presentation by APC cells, as well as the proliferation and differentiation of B cells (Figure S8A). We also identified potential relationships and crosstalk between the differentially expressed proteins in plasma and urine, respectively (Figures S8B and S8C).

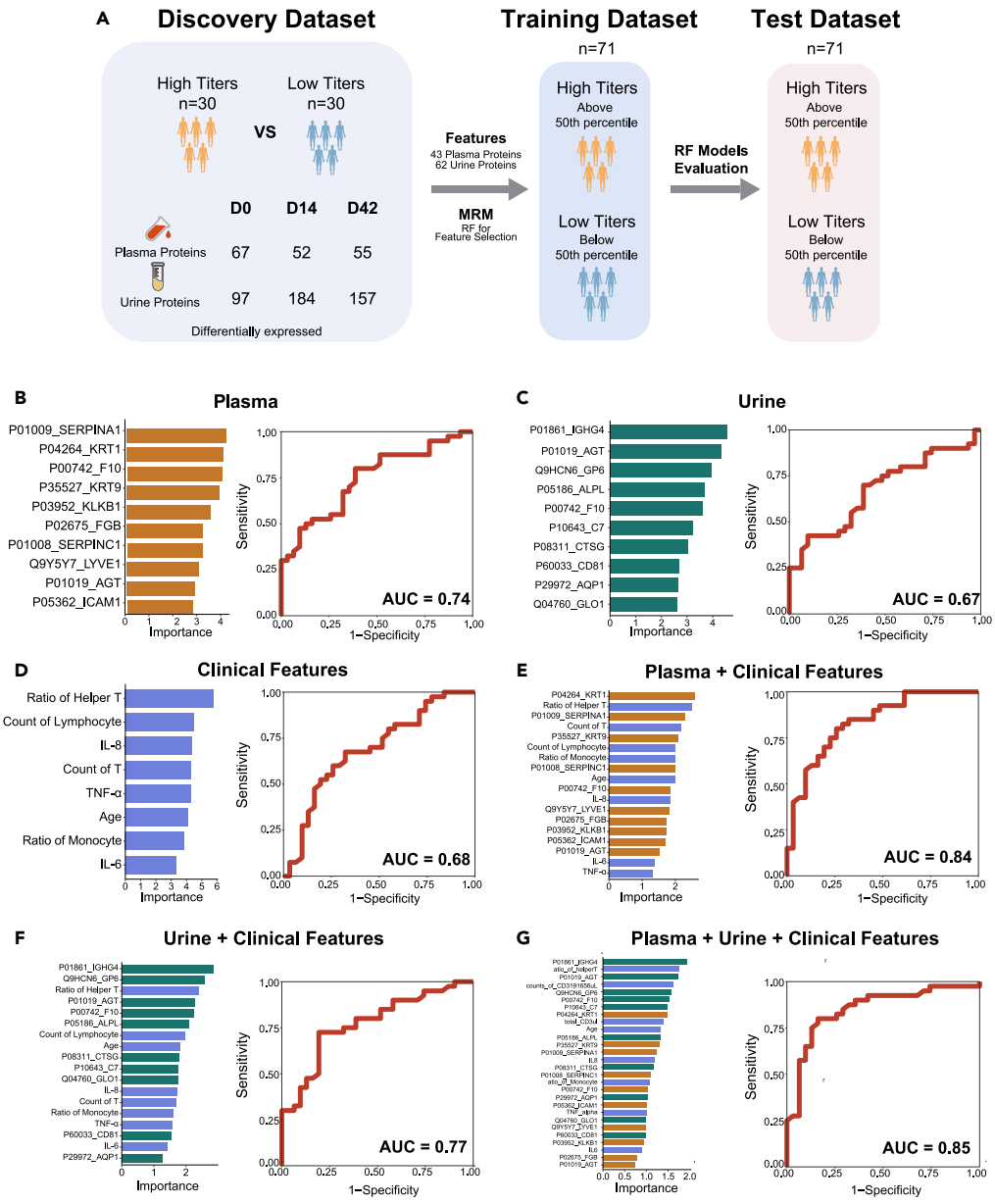

Figure 6. Predictive model for vaccination responses using the integration of proteomic data before vaccination

(A) Workflow for the construction of the prediction model. 60 participants with both plasma and urine proteomic data were considered as the discovery cohort. An additional 71 independent participants were recruited as a training cohort, and another 71 participants were recruited as a test cohort.

(B) Ten plasma proteins were selected to build a 10-molecule model, and the area under curve (AUC) value was calculated.

(C) Ten urine proteins were selected to construct a 10-molecule model, and the AUC value was calculated.

(D) Eight clinical features were selected for constructing an 8-molecule model, and the AUC value was calculated.

(E) Combination of plasma and clinical features for the construction of the prediction model.

(F) Combination of urine and clinical features for the construction of the prediction model.

(G) Combination of the plasma, urine, and clinical features for constructing the prediction model.

DISCUSSION

In this study, we investigated the dynamics of plasma and urine proteome after vaccination to understand the different vaccination responses to COVID-19. Our results showed that dysregulated proteins in the plasma after vaccination were involved in various biological processes such as detoxification of reactive oxygen species, and immunocyte chemotaxis (Figures 2A–2C). On the other hand, dysregulated urine proteins were related to immunocyte chemotaxis (Figures 2D and 2E).

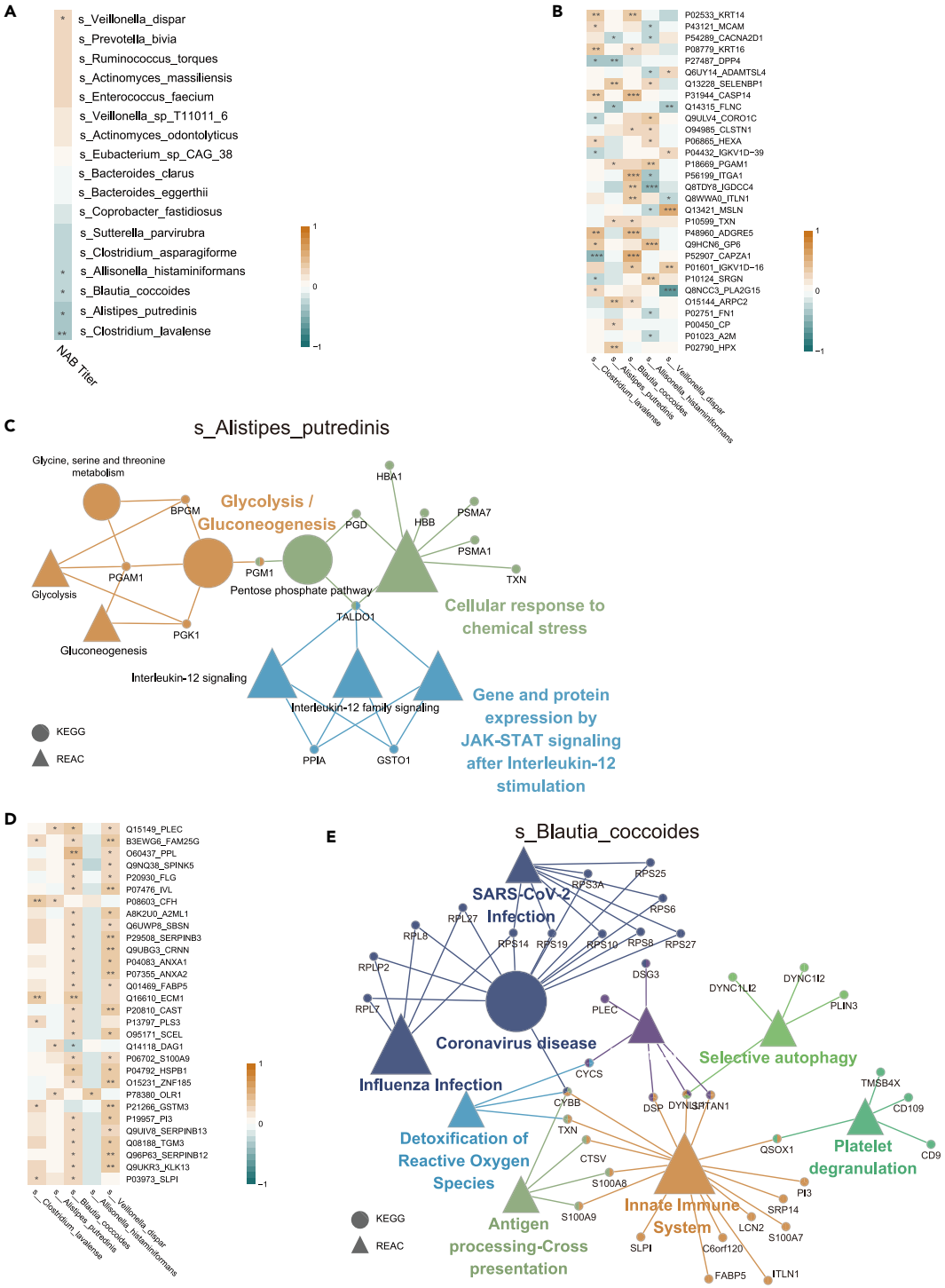

Figure 7. Correlation between the enriched bacteria and plasma and urine proteins

(A) Correlation heatmap of differentially enriched bacteria at D0 with the ACE2-RBD-inhibiting antibody titers (n = 60, Spearman correlation, *p < 0.05, **p < 0.01).

(B) Correlation between the enriched bacteria and plasma proteins. *p* values were calculated by Pearson correlation analysis (*p < 0.05, **p < 0.01, ***p < 0.001).

(C) KEGG and REAC analysis of the proteins correlated with *Alistipes putredinis* abundance in plasma.

(D) Correlation between the enriched bacteria and urine proteins. *p* values were calculated by Pearson correlation analysis (*p < 0.05, **p < 0.01, ***p < 0.001).

(E) KEGG and REAC analysis of the proteins correlated with *Blautia coccoides* abundance in urine.

ROS typically influences DC function in manifold aspects by regulating cytokine production, maturation, migration and antigen presentation.[36] In the process of DCs during cross-presentation to cytotoxic $CD8^+$ T cells, NADPH oxidases 2 (NOX2) is recruited into phagosome resulting in an alkalization of its content through the production of low level ROS leading to structural preservation of the internalized antigens, and allows its successful presentation via the MHC I complex.[36] ROS is a requisite secondary signaling factor in T cell immunity. TCR stimulation induces the generation of an enormous amount of ROS, thus resulting in the activation of nuclear factor of activated T cells (NFAT) and NF-kB, leading to activating of T cells.[37] For the immunocyte chemotaxis, chemokine and receptor expression coordinates the migration of antigen-loaded DCs from tissues into lymphoid tissue to activate T and B cells to initiate the adaptive immune response.[38–40] The CC (α-chemokines) and the CXC (β-chemokines) families of chemokines play a crucial role in host immunity to viral infections and serve as the surrogates of vaccine-induced innate and adaptive protective responses, facilitating the improvement of vaccine efficacy.[41]

Moreover, the plasma proteomics revealed that the LXR/RXR activation was associated with the production of ACE2-RBD-inhibiting antibodies. LXR/RXR heterodimer enhanced the expression of antiapoptotic regulators and inhibiting the expression of proapoptotic regulator.[42] Furthermore, LXR agonist-programmed DCs increased the myeloid DC differentiation and shows a stronger capacity for stimulate T cell proliferation.[43] Moreover, activation of LXRs can improve the efficacy of cytotoxic T lymphocyte.[44]

The urine proteomics showed that complement system, acute phase response signaling, LXR/RXR, FXR/RXR, and STAT3 pathways were correlated with the NAB production. The complement system is composed of more than 30 serum proteins and cell surface receptors facilitating pathogen elimination by opsonizing pathogens, promoting chemotaxis of immune cells or directly damaging pathogen surfaces.[45] C3a and C5a are able to bind to their respective receptors on the T cell membrane, thereby stimulating effector function and maintaining T cell viability.[46] CR3 and CR2 capture antigens forming CR3-CR2-iC3b-antigen complexes and present to antigen specific B cell receptors modulating B cell signaling.[47] Acute Phase Response (APR) functions facilitated by IL-6 include the maturation of B and T cells and hematopoiesis.[48] FXR is a bile acid activated nuclear receptor (BAR). The secondary bile acid 3β-hydroxydeoxycholic acid (isoDCA) increased immunosuppressive $CD4^+$ regulatory T (Treg) cells by diminishing immunostimulatory activity of dendritic cells (DCs), which depended on inhibition of FXR signaling in DCs.[49] STAT3 present in the cytoplasm in an inactive form and can be stimulated by a vast range of cytokines, chemokines and growth factors. Numerous reports indicate STAT3 affects DC maturation and activation. Flt3L-Flt3-STAT3 pathway promotes pDC generation from CDPs via direct induction of *Tcf4*.[50] Repression of DC maturation/function can be achieved via IL-6-STAT3 or IL-10-STAT3-mediated signaling directly, or indirectly through inhibitory molecules that induce IL-6. Overall, the above signaling pathway profoundly affect host immunity, thereby affecting the production of neutralizing antibodies.

To achieve data integration, three matrices containing differential plasma proteins, urine proteins and clinical features were merged as a whole matrix, which was utilized for feature selection and model construction. In detail, Random Forest was used to construct the predictive models based on the whole matrix after the selection of the features according to their Gini importance. By integrating dysregulated proteins in plasma and urine, as well as clinical features collected before vaccination, we developed a model for predicting vaccination responses with an AUC value of 0.85, as summarized in the Graphic Abstract. The development of models for predicting vaccination response helps us understand the immunological processes and contributes to improving therapeutics. The baseline immune profiles have been demonstrated to predict different vaccine responses.[10–12] Further studies showed that $CD20^+CD38{+}{+}$ B cell signature could predict immune responsiveness in independent influenza datasets.[51] This signature was associated with typeIIFN responses and activation of dendritic cells. Signaling pathways such as JAK-STAT and interleukin signaling, Toll-like receptor cascades, interferon signaling, and Th17 cell differentiation were important HBV pre-vaccination modulators.[52] Interestingly, the peripheral blood monocyte-to-lymphocyte ratios at baseline were a predictive parameter to assess the response to malaria vaccination.[53] All the above studies indicate the possibility to improve the vaccination outcome by modulating the immune baseline. Differential antibody responses to inactivated and mRNA vaccines against SARS-Cov-2 have been observed.[54,55] However, the mechanisms that determine the quality and quantity of these responses are largely unknown.[54,55] The immune responses following vaccination with the BNT162b2 mRNA vaccine showed lower interferon-γ and interleukin-2 production in older participants.[56] Lower lymphocyte count and higher serum SAA level have been reported to be correlated with lower seroconversion rate to inactivated COVID-19 vaccines.[55] In this study, we integrated plasma, urine proteomic data, and clinical features before vaccination, which could provide a novel strategy for improving COVID-19 vaccine efficacy.

Several studies of COVID-19 plasma samples have identified multiple dysregulated proteins and metabolites in severe cases compared with non-severe cases.[57] However, few studies have been reported to investigate the correlation between plasma proteomics and antibody response. The innate immune response is enhanced in severe patients, involving the activation of acute phase proteins and the complement system. Our study showed that the high-response group's complement system was also dysregulated (Figures 3 and 4). Our results show that the LXR/RXR activation was associated with the production of ACE2-RBD-inhibiting antibodies (Figures 3 and 4). It has been reported that LXR agonists induced the expression of antiapoptotic regulators, and inhibited proapoptotic regulators and effectors, leading to inhibition of macrophage apoptosis.[58] LXR agonists promoted DC maturation and IL-12, TNF-a, IL-6, and IL-8 production and enhanced the capacity of DCs to induce $CD4^+$ T cell proliferation.[42] LXR agonists may serve as new potential targets for enhancing the COVID-19 vaccine response.

Overall, this study presents a comprehensive proteomic analysis of plasma and urine samples from participants receiving BBIBP-CorV vaccine. We have developed a model for predicting the neutralizing antibody response based on the baseline proteins and clinical characteristics. Modulating immune status at the baseline may provide a novel strategy for enhancing COVID-19 vaccine efficacy.

Limitations of the study

There are several limitations in this study. First, this single-center study with a relatively small size of participants lacks external validation. Second, we observed the correlations between vaccine response and plasma and urine proteomics change at D0, D14, and D42. A longer follow-up of observation could be carried out to support our conclusion. Moreover, a molecular mechanism study should be carried out to clarify the cause-and-effect relationship between vaccine response and changes in plasma and urine proteomics. Overall, this study indicates that modulating immune status at the baseline may provide a novel strategy for enhancing COVID-19 efficacy.

STAR★METHODS

Detailed methods are provided in the online version of this paper and include the following:

- KEY RESOURCES TABLE
- RESOURCE AVAILABILITY
  - Lead contact
  - Materials availability
  - Data and code availability
- EXPERIMENTAL MODEL AND STUDY PARTICIPANT DETAILS
  - Experimental design, plasma and urine sample collection from healthy volunteers
- METHODS DETAILS
  - Detection of the ACE2-RBD-inhibiting antibody, blood routine and cytokines
  - Peptide preparation for proteomic analysis
  - MRM analysis in the training and test cohorts
  - Quality control
  - Mufzz and pathway analysis
  - Cytokine analysis
  - Random forest analysis
  - Fecal genomic DNA extraction and metagenomic sequencing and data analysis
  - Database search
- QUANTIFICATION AND STATISTICAL ANALYSIS
- ADDITIONAL RESOURCES

SUPPLEMENTAL INFORMATION

Supplemental information can be found online at https://doi.org/10.1016/j.isci.2024.108851.

ACKNOWLEDGMENTS

This work was supported by Key Project of National Science Foundation of Chinaation of China (82030020), National Key R&D Program of China (2021YFA1301602), China Postdoctoral Science Foundation (2021TQ0283), International Postdoctoral Exchange Fellowship Program (Talent-Introduction Program, YJ20210170), Westlake Education Foundation, Science and Technology Innovation Enhancement Project of Army Medical University (STIEP 2021XQN20). We thank Westlake University Supercomputer Center for assistance in data generation and storage, and the Mass Spectrometry & Metabolomics Core Facility at the Center for Biomedical Research Core Facilities of Westlake University for sample analysis.

AUTHOR CONTRIBUTIONS

Conceptualization, S.Y., T.G., and Z.L.; methodology, Z.D., X.J., and Q.B.; software, H.W., L.T., and Q.B.; formal analysis, C.H. and W.H.; investigation, C.H., W.H., B.T., X.J., H.W., L.H., M.L., Y.X., C.L., X.L.,Y.L., J.L., and G.H.; resources, B.T. and W.H.; data curation, Z.D. and Q.B.; writing–original draft, C.H. and W.H.; writing–review and editing, S.Y., T.G., Z.D., and Z.L; supervision, S.Y., T.G., Z.D., and Z.L; funding acquisition, S.Y., C.H., T.G., and Z.D.

DECLARATION OF INTERESTS

The authors declare that there is no conflict of interest.

Received: April 14, 2023
Revised: October 15, 2023
Accepted: January 3, 2024
Published: January 8, 2024

REFERENCES

1. Zhang, Q., Bastard, P., COVID Human Genetic Effort, Cobat, A., and Casanova, J.L. (2022). Human genetic and immunological determinants of critical COVID-19 pneumonia. Nature *603*, 587–598.
2. Merad, M., Blish, C.A., Sallusto, F., and Iwasaki, A. (2022). The immunology and immunopathology of COVID-19. Science *375*, 1122–1127.
3. Barda, N., Dagan, N., Cohen, C., Hernán, M.A., Lipsitch, M., Kohane, I.S., Reis, B.Y., and Balicer, R.D. (2021). Effectiveness of a third dose of the BNT162b2 mRNA COVID-19 vaccine for preventing severe outcomes in Israel: an observational study. Lancet *398*, 2093–2100.
4. Krause, P.R., Fleming, T.R., Peto, R., Longini, I.M., Figueroa, J.P., Sterne, J.A.C., Cravioto, A., Rees, H., Higgins, J.P.T., Boutron, I., et al. (2021). Considerations in boosting COVID-19 vaccine immune responses. Lancet *398*, 1377–1380.
5. Hall, V.J., Foulkes, S., Saei, A., Andrews, N., Oguti, B., Charlett, A., Wellington, E., Stowe, J., Gillson, N., Atti, A., et al. (2021). COVID-19 vaccine coverage in health-care workers in England and effectiveness of BNT162b2 mRNA vaccine against infection (SIREN): a prospective, multicentre, cohort study. Lancet *397*, 1725–1735.
6. Altmann, D.M., and Boyton, R.J. (2022). COVID-19 vaccination: The road ahead. Science *375*, 1127–1132.
7. Bertoglio, F., Fühner, V., Ruschig, M., Heine, P.A., Abassi, L., Klünemann, T., Rand, U., Meier, D., Langreder, N., Steinke, S., et al. (2021). A SARS-CoV-2 neutralizing antibody selected from COVID-19 patients binds to the ACE2-RBD interface and is tolerant to most known RBD mutations. Cell Rep. *36*, 109433.
8. Feikin, D.R., Higdon, M.M., Abu-Raddad, L.J., Andrews, N., Araos, R., Goldberg, Y., Groome, M.J., Huppert, A., O'Brien, K.L., Smith, P.G., et al. (2022). Duration of effectiveness of vaccines against SARS-CoV-2 infection and COVID-19 disease: results of a systematic review and meta-regression. Lancet *399*, 924–944.
9. Wang, Y., Wang, X., Luu, L.D.W., Chen, S., Jin, F., Wang, S., Huang, X., Wang, L., Zhou, X., Chen, X., et al. (2022). Proteomic and Metabolomic Signatures Associated With the Immune Response in Healthy Individuals Immunized With an Inactivated SARS-CoV-2 Vaccine. Front. Immunol. *13*, 848961.
10. Tsang, J.S., Dobaño, C., VanDamme, P., Moncunill, G., Marchant, A., Othman, R.B., Sadarangani, M., Koff, W.C., and Kollmann, T.R. (2020). Improving Vaccine-Induced Immunity: Can Baseline Predict Outcome? Trends Immunol. *41*, 457–465.
11. Tsang, J.S., Schwartzberg, P.L., Kotliarov, Y., Biancotto, A., Xie, Z., Germain, R.N., Wang, E., Olnes, M.J., Narayanan, M., Golding, H., et al. (2014). Global analyses of human immune variation reveal baseline predictors of postvaccination responses. Cell *157*, 499–513.
12. Fourati, S., Cristescu, R., Loboda, A., Talla, A., Filali, A., Railkar, R., Schaeffer, A.K., Favre, D., Gagnon, D., Peretz, Y., et al. (2016). Pre-vaccination inflammation and B-cell signalling predict age-related hyporesponse to hepatitis B vaccination. Nat. Commun. *7*, 10369.
13. Warimwe, G.M., Fletcher, H.A., Olotu, A., Agnandji, S.T., Hill, A.V.S., Marsh, K., and Bejon, P. (2013). Peripheral blood monocyte-to-lymphocyte ratio at study enrollment predicts efficacy of the RTS,S malaria vaccine: analysis of pooled phase II clinical trial data. BMC Med. *11*, 184.
14. Bi, X., Liu, W., Ding, X., Liang, S., Zheng, Y., Zhu, X., Quan, S., Yi, X., Xiang, N., Du, J., et al. (2022). Proteomic and metabolomic profiling of urine uncovers immune responses in patients with COVID-19. Cell Rep. *38*, 110271.
15. Shen, B., Yi, X., Sun, Y., Bi, X., Du, J., Zhang, C., Quan, S., Zhang, F., Sun, R., Qian, L., et al. (2020). Proteomic and Metabolomic Characterization of COVID-19 Patient Sera. Cell *182*, 59–72.e15.
16. Messner, C.B., Demichev, V., Wendisch, D., Michalick, L., White, M., Freiwald, A., Textoris-Taube, K., Vernardis, S.I., Egger, A.S., Kreidl, M., et al. (2020). Ultra-High-Throughput Clinical Proteomics Reveals Classifiers of COVID-19 Infection. Cell Syst. *11*, 11–24.e4.
17. Findeisen, H.M., Voges, V.C., Braun, L.C., Sonnenberg, J., Schwarz, D., Körner, H., Reinecke, H., and Sohrabi, Y. (2022). LXRα Regulates oxLDL-Induced Trained Immunity in Macrophages. Int. J. Mol. Sci. *23*, 6166.
18. Haraldsson, B., Nyström, J., and Deen, W.M. (2008). Properties of the glomerular barrier and mechanisms of proteinuria. Physiol. Rev. *88*, 451–487.
19. Muir, L.A., Cho, K.W., Geletka, L.M., Baker, N.A., Flesher, C.G., Ehlers, A.P., Kaciroti, N., Lindsly, S., Ronquist, S., Rajapakse, I., et al. (2022). Human CD206+ macrophages associate with diabetes and adipose tissue lymphoid clusters. JCI Insight *7*, e146563.
20. Lok, L.S.C., and Clatworthy, M.R. (2021). Neutrophils in secondary lymphoid organs. Immunology *164*, 677–688.
21. Seliga, A., Lee, M.H., Fernandes, N.C., Zuluaga-Ramirez, V., Didukh, M., Persidsky, Y., Potula, R., Gallucci, S., and Sriram, U. (2018). Kallikrein-Kinin System Suppresses Type I Interferon Responses: A Novel Pathway of Interferon Regulation. Front. Immunol. *9*, 156.
22. Tavazoie, M.F., Pollack, I., Tanqueco, R., Ostendorf, B.N., Reis, B.S., Gonsalves, F.C., Kurth, I., Andreu-Agullo, C., Derbyshire, M.L., Posada, J., et al. (2018). LXR/ApoE Activation Restricts Innate Immune Suppression in Cancer. Cell *172*, 825–840.e18.
23. Tang, X., Sun, R., Ge, W., Mao, T., Qian, L., Huang, C., Kang, Z., Xiao, Q., Luo, M., Zhang, Q., et al. (2022). Enhanced inflammation and suppressed adaptive immunity in COVID-19 with prolonged RNA shedding. Cell Discov. *8*, 70.
24. Fiorucci, S., Zampella, A., Ricci, P., Distrutti, E., and Biagioli, M. (2022). Immunomodulatory functions of FXR. Mol. Cell. Endocrinol. *551*, 111650.
25. Wu, D., Shu, T., Yang, X., Song, J.X., Zhang, M., Yao, C., Liu, W., Huang, M., Yu, Y., Yang, Q., et al. (2020). Plasma metabolomic and lipidomic alterations associated with COVID-19. Natl. Sci. Rev. *7*, 1157–1168.
26. Lazzaroni, M.G., Piantoni, S., Masneri, S., Garrafa, E., Martini, G., Tincani, A., Andreoli, L., and Franceschini, F. (2021). Coagulation dysfunction in COVID-19: The interplay between inflammation, viral infection and the coagulation system. Blood Rev. *46*, 100745.
27. Jafarzadeh, A., Nemati, M., and Jafarzadeh, S. (2021). Contribution of STAT3 to the pathogenesis of COVID-19. Microb. Pathog. *154*, 104836.
28. Cao, Y., Su, B., Guo, X., Sun, W., Deng, Y., Bao, L., Zhu, Q., Zhang, X., Zheng, Y., Geng, C., et al. (2020). Potent Neutralizing Antibodies against SARS-CoV-2 Identified by High-Throughput Single-Cell Sequencing of Convalescent Patients' B Cells. Cell *182*, 73–84.e16.
29. Hughes, T., Hansson, L., Akkouh, I., Hajdarevic, R., Bringsli, J.S., Torsvik, A., Inderhaug, E., Steen, V.M., and Djurovic, S. (2020). Runaway multi-allelic copy number variation at the alpha-defensin locus in African and Asian populations. Sci. Rep. *10*, 9101.
30. Shrivastava, S., Chelluboina, S., Jedge, P., Doke, P., Palkar, S., Mishra, A.C., and Arankalle, V.A. (2021). Elevated Levels of Neutrophil Activated Proteins, Alpha-Defensins (DEFA1), Calprotectin (S100A8/A9) and Myeloperoxidase (MPO) Are Associated With Disease Severity in COVID-19 Patients. Front. Cell. Infect. Microbiol. *11*, 751232.
31. Liu, L.Z., Zhang, Z., Zheng, B.H., Shi, Y., Duan, M., Ma, L.J., Wang, Z.C., Dong, L.Q., Dong, P.P., Shi, J.Y., et al. (2019). CCL15 Recruits Suppressive Monocytes to Facilitate Immune Escape and Disease Progression in Hepatocellular Carcinoma. Hepatology *69*, 143–159.
32. Mantovani, A., Dinarello, C.A., Molgora, M., and Garlanda, C. (2019). Interleukin-1 and Related Cytokines in the Regulation of Inflammation and Immunity. Immunity *50*, 778–795.
33. Costela-Ruiz, V.J., Illescas-Montes, R., Puerta-Puerta, J.M., Ruiz, C., and Melguizo-Rodríguez, L. (2020). SARS-CoV-2 infection: The role of cytokines in COVID-19 disease. Cytokine Growth Factor Rev. *54*, 62–75.
34. Lynn, D.J., Benson, S.C., Lynn, M.A., and Pulendran, B. (2022). Modulation of immune responses to vaccination by the microbiota: implications and potential mechanisms. Nat. Rev. Immunol. *22*, 33–46.
35. Hagan, T., Cortese, M., Rouphael, N., Boudreau, C., Linde, C., Maddur, M.S., Das, J., Wang, H., Guthmiller, J., Zheng, N.Y., et al. (2019). Antibiotics-Driven Gut Microbiome Perturbation Alters Immunity to Vaccines in Humans. Cell *178*, 1313–1328.e13.
36. Savina, A., Jancic, C., Hugues, S., Guermonprez, P., Vargas, P., Moura, I.C., Lennon-Duménil, A.M., Seabra, M.C., Raposo, G., and Amigorena, S. (2006). NOX2 controls phagosomal pH to regulate antigen processing during crosspresentation by dendritic cells. Cell *126*, 205–218.
37. Peng, H.Y., Lucavs, J., Ballard, D., Das, J.K., Kumar, A., Wang, L., Ren, Y., Xiong, X., and Song, J. (2021). Metabolic Reprogramming and Reactive Oxygen Species in T Cell Immunity. Front. Immunol. *12*, 652687.
38. Coelho, A.L., Hogaboam, C.M., and Kunkel, S.L. (2005). Chemokines provide the sustained inflammatory bridge between innate and acquired immunity. Cytokine Growth Factor Rev. *16*, 553–560.
39. Liu, J., Zhang, X., Cheng, Y., and Cao, X. (2021). Dendritic cell migration in inflammation and immunity. Cell. Mol. Immunol. *18*, 2461–2471.
40. Lu, Y., and You, J. (2023). Strategy and application of manipulating DCs chemotaxis

in disease treatment and vaccine design. Biomed. Pharmacother. *161*, 114457.

41. Karimabad, M.N., Hassanshahi, G., Kounis, N.G., Mplani, V., Roditis, P., Gogos, C., Lagadinou, M., Assimakopoulos, S.F., Dousdampanis, P., and Koniari, I. (2022). The Chemokines CXC, CC and C in the Pathogenesis of COVID-19 Disease and as Surrogates of Vaccine-Induced Innate and Adaptive Protective Responses. Vaccines (Basel) *10*, 1299.
42. Kiss, M., Czimmerer, Z., and Nagy, L. (2013). The role of lipid-activated nuclear receptors in shaping macrophage and dendritic cell function: From physiology to pathology. J. Allergy Clin. Immunol. *132*, 264–286.
43. Zhong, L., Yang, Q., Xie, W., and Zhou, J. (2014). Liver X receptor regulates mouse GM-CSF-derived dendritic cell differentiation *in vitro*. Mol. Immunol. *60*, 32–43.
44. Bilotta, M.T., Petillo, S., Santoni, A., and Cippitelli, M. (2020). Liver X Receptors: Regulators of Cholesterol Metabolism, Inflammation, Autoimmunity, and Cancer. Front. Immunol. *11*, 584303.
45. Cummings, K.L., Waggoner, S.N., Tacke, R., and Hahn, Y.S. (2007). Role of complement in immune regulation and its exploitation by virus. Viral Immunol. *20*, 505–524.
46. Cravedi, P., Leventhal, J., Lakhani, P., Ward, S.C., Donovan, M.J., and Heeger, P.S. (2013). Immune cell-derived C3a and C5a costimulate human T cell alloimmunity. Am. J. Transplant. *13*, 2530–2539.
47. Kareem, S., Jacob, A., Mathew, J., Quigg, R.J., and Alexander, J.J. (2023). Complement: Functions, location and implications. Immunology *170*, 180–192.
48. Bresnahan, K.A., and Tanumihardjo, S.A. (2014). Undernutrition, the acute phase response to infection, and its effects on micronutrient status indicators. Adv. Nutr. *5*, 702–711.
49. Campbell, C., McKenney, P.T., Konstantinovsky, D., Isaeva, O.I., Schizas, M., Verter, J., Mai, C., Jin, W.B., Guo, C.J., Violante, S., et al. (2020). Bacterial metabolism of bile acids promotes generation of peripheral regulatory T cells. Nature *581*, 475–479.
50. Hillmer, E.J., Zhang, H., Li, H.S., and Watowich, S.S. (2016). STAT3 signaling in immunity. Cytokine Growth Factor Rev. *31*, 1–15.
51. Kotliarov, Y., Sparks, R., Martins, A.J., Mulè, M.P., Lu, Y., Goswami, M., Kardava, L., Banchereau, R., Pascual, V., Biancotto, A., et al. (2020). Broad immune activation underlies shared set point signatures for vaccine responsiveness in healthy individuals and disease activity in patients with lupus. Nat. Med. *26*, 618–629.
52. Shannon, C.P., Blimkie, T.M., Ben-Othman, R., Gladish, N., Amenyogbe, N., Drissler, S., Edgar, R.D., Chan, Q., Krajden, M., Foster, L.J., et al. (2020). Multi-Omic Data Integration Allows Baseline Immune Signatures to Predict Hepatitis B Vaccine Response in a Small Cohort. Front. Immunol. *11*, 578801.
53. Antwi-Baffour, S., Kyeremeh, R., Buabeng, D., Adjei, J.K., Aryeh, C., Kpentey, G., and Seidu, M.A. (2018). Correlation of malaria parasitaemia with peripheral blood monocyte to lymphocyte ratio as indicator of susceptibility to severe malaria in Ghanaian children. Malar. J. *17*, 419.
54. Bergamaschi, C., Terpos, E., Rosati, M., Angel, M., Bear, J., Stellas, D., Karaliota, S., Apostolakou, F., Bagratuni, T., Patseas, D., et al. (2021). Systemic IL-15, IFN-gamma, and IP-10/CXCL10 signature associated with effective immune response to SARS-CoV-2 in BNT162b2 mRNA vaccine recipients. Cell Rep. *36*, 109504.
55. Zhang, J., Xing, S., Liang, D., Hu, W., Ke, C., He, J., Yuan, R., Huang, Y., Li, Y., Liu, D., et al. (2021). Differential Antibody Response to Inactivated COVID-19 Vaccines in Healthy Subjects. Front. Cell. Infect. Microbiol. *11*, 791660.
56. Collier, D.A., Ferreira, I.A.T.M., Kotagiri, P., Datir, R.P., Lim, E.Y., Touizer, E., Meng, B., Abdullahi, A.; CITIID-NIHR BioResource COVID-19 Collaboration, and Elmer, A., et al. (2021). Age-related immune response heterogeneity to SARS-CoV-2 vaccine BNT162b2. Nature *596*, 417–422.
57. Rahimi, A., Mirzazadeh, A., and Tavakolpour, S. (2021). Genetics and genomics of SARS-CoV-2: A review of the literature with the special focus on genetic diversity and SARS-CoV-2 genome detection. Genomics *113*, 1221–1232.
58. Valledor, A.F., Hsu, L.C., Ogawa, S., Sawka-Verhelle, D., Karin, M., and Glass, C.K. (2004). Activation of liver X receptors and retinoid X receptors prevents bacterial-induced macrophage apoptosis. Proc. Natl. Acad. Sci. USA *101*, 17813–17818.
59. Krämer, A., Green, J., Pollard, J., Jr., and Tugendreich, S. (2014). Causal analysis approaches in Ingenuity Pathway Analysis. Bioinformatics *30*, 523–530.
60. Kveler, K., Starosvetsky, E., Ziv-Kenet, A., Kalugny, Y., Gorelik, Y., Shalev-Malul, G., Aizenbud-Reshef, N., Dubovik, T., Briller, M., Campbell, J., et al. (2018). Immune-centric network of cytokines and cells in disease context identified by computational mining of PubMed. Nat. Biotechnol. *36*, 651–659.
61. Yu, Y., Ouyang, Y., and Yao, W. (2018). shinyCircos: an R/Shiny application for interactive creation of Circos plot. Bioinformatics *34*, 1229–1231.

STAR★METHODS

KEY RESOURCES TABLE

REAGENT or RESOURCE	SOURCE	IDENTIFIER
Biological samples		
Plasma samples	Xinqiao Hospital	This paper (Tables S1, S2, and S3)
Urine samples	Xinqiao Hospital	This paper (Tables S1, S2, and S3)
Stool samples	Xinqiao Hospital	This paper (Tables S1, S2, and S3)
Chemicals, peptides, and recombinant proteins		
Acetone	Sigma-aldrich	80000367
Sodium hydroxide	Sigma-aldrich	221465-500g
Triethylammonium bicarbonate buffer (TEAB)	Sigma-aldrich	T7408-500ML
Urea	Sigma-aldrich	U1250-1KG
Tris	Solarbio	T8060
Tris (2-carboxyethyl) phosphine (TCEP)	AdamasReagentd	61820E
Iodoacetamide (IAA)	Sigma-aldrich	I6125-25G
Trypsin	Hualishi Scientific	HLS TRY001C-100μg
Trifluoroacetic acid (TFA)	Thermo Fisher Scientific	T/3258/PB05CN
Methanol	Thermo Fisher Scientific	A452-4
Acetonitrile (ACN)	Thermo Fisher Scientific	A955-4
Formic acid (FA)	Thermo Fisher Scientific	A955-4
TMTPRO 16-PLEX	Thermo Fisher Scientific	A44520
50% Hydroxylamine	Thermo Fisher Scientific	90115
Ammonium hydroxide solution	Sigma-aldrich	221228-2.5L-A
MS grade water	Thermo Fisher Scientific	W6-4
NaOH	Sigma-aldrich	221465-500g
3 KDa, 0.5 mL ultrafilter	Merck Millipore	UFC500396
SOLAμ	Thermo Fisher Scientific	62209-001
Critical commercial assays		
TMTpro 16plex reagents	Thermo Fisher Scientific	A44520
High SelectTM Top-14 Abundant Protein Depletion Mini Spin Columns	Thermo Fisher Scientific	A36370
TIANamp Stool DNA Kit	TIANGEN	DP328
Deposited data		
The raw data of Mass spectrometry	https://www.iprox.org	IPX0004618000
Raw sequencing data	https://ngdc.cncb.ac.cn/gsa/	CRA007947
Data analysis codes	zenodo.org	https://doi.org/10.5281/zenodo.5642579
Software and algorithms		
R software environment (version 4.2.2)	R Project	https://cran.r-project.org/
Cytoscape (version 3.9.1)	Open-source	https://cytoscape.org/
HIPLOT	Open-source	https://hiplot-academic.com/
shinyCircos	Open-source	https://yimingyu.shinyapps.io/shinycircos/
Xcalibur	Thermo Fisher Scientific	OPTON-30965
Proteome Discoverer (version 2.4.1.15)	Thermo Fisher Scientific	N/A
Ingenuine Pathway Analysis	QIAGEN Digital Insights	N/A

(*Continued on next page*)

Continued

REAGENT or RESOURCE	SOURCE	IDENTIFIER
IMMPORT	Northrop Grumman Information Technology Health Solutions	https://www.immport.org/
UniProt	Open-source	https://www.uniprot.org/
STRING	Open-source	https://www.string-db.org/
GraphPad Prism	GraphPad Software	Version 9.0
Other		
Sep-Pak C18 Vac cartridges (50 mg)	Waters	WAT054955
XBridge Peptide BEH C18 column (300 Å, 5 μm, 4.6 mm x 250 mm)	Waters	186003625
Chinese Clinical Trial Registry	https://www.chictr.org.cn/showproj.html?proj=122521	ChiCTR2100044919

RESOURCE AVAILABILITY

Lead contact

Further information and requests for resources and reagents should be directed to and will be fulfilled by the lead contact, Shiming Yang (yangshiming@tmmu.edu.cn).

Materials availability

This study did not generate new unique reagents.

Data and code availability

- Raw and processed mass spectrometry proteomic data generated in this study are available at iProx (https://www.iprox.cn/page/home.html) with the project ID IPX0004618000. Raw sequencing data was deposited at National Genomics Data Center (https://ngdc.cncb.ac.cn/gsa/) and available via the accession number CRA007947.
- This paper does not report original code. The R code can be downloaded from https://doi.org/10.5281/zenodo.5642579.
- Any additional information required to reanalyze the data reported in this work is available from the lead contact upon reasonable request.

EXPERIMENTAL MODEL AND STUDY PARTICIPANT DETAILS

Experimental design, plasma and urine sample collection from healthy volunteers

In this study, 60 healthy volunteers (Discovery Cohort) were first recruited by the Department of Gastroenterology of Xinqiao Hospital, Chongqing, and vaccinated with two doses of the BBIBP-CorV vaccine (Beijing Institute of Biological Products Co., Ltd.) between February 1 and July 18, 2021. During the same period, an independent 71 healthy volunteers (training cohort) and another 71 healthy volunteers (test cohort) were also recruited for vaccination administration. This study was approved by the Ethics Committee of Westlake University and Xinqiao Hospital of Third Military Medical University and was registered at the Chinese Clinical Trial Registry (ChiCTR2100044919). The methodologies conformed to the standards of the Declaration of Helsinki. Participants met the following inclusion criteria: (1) age between 18-60, with good physical health based on medical history and physical examination; (2) seronegative for IgM/IgG antibodies against SARS-CoV-2; (3) completed the whole research procedure and provided the plasma and urine samples at the indicated times. A written informed consent form was signed prior to the trial. The exclusion criteria were as follows: (1) allergy to any ingredient of the vaccine; (2) severe allergic reactions to vaccines in the past (such as acute allergic reactions, angioedema, or dyspnea, etc.); (3) any chronic disease (such as heart disease, cancer, diabetes, respiratory conditions, arthritis, and kidney disease, etc.); (4) any autoimmune disease (including Guillain-Barré syndrome, autoimmune hemolytic anemia, and Graves' disease, etc.); (5) those who have a fever, or suffer from acute diseases, or acute attacks of chronic diseases and (6) pregnant women. All the participants received two doses of BBIBP-CorV vaccination (Day 0 and Day 28) (Beijing Institute of Biological Products Co., Ltd.). Plasma and urine were collected from all the participants on Day 0, Day 14, and Day 42 for assays of NAB titers, routine blood tests, inflammatory cytokines, and proteomics. Stool samples were collected for metagenomic sequencing. The plasma and urine proteins derived from 60 healthy volunteers (Discovery Cohort) with gender balance were submitted for tandem mass tags (TMT)-labeled quantitative proteomics, while the plasma and urine proteins derived from 71 healthy volunteers (training cohort) and another 71 healthy volunteers (test cohort) were subjected to multiple reaction monitoring (MRM)-based targeted mass spectrometry.

METHODS DETAILS

Detection of the ACE2-RBD-inhibiting antibody, blood routine and cytokines

All the plasma samples were inactivated at 56°C for 45 min before testing. The ACE2-RBD inhibiting antibody levels were detected by commercial MCLIA kits (Bioscience, China). Briefly, 20 μL plasma samples were preincubated with 40 μL recombinant RBD of SARS-CoV-2 conjugated with alkaline phosphatase. Subsequently, 20 μL of recombinant ACE2-coated magnetic beads were added to the above mixture. Then, the chemiluminescent substrate was added to the mixture, and the relative light units (RLU) were qualitatively measured by an automated magnetic chemiluminescence analyzer (Axceed 260, Bioscience, China). The levels of the ACE2-RBD-inhibiting antibody were finally calculated according to the standard curves. C-reactive protein (CRP) was determined by a quantitative immune analyzer (FIA8600, Getein Biotech, Nanjing, China). The routine blood test, including hemoglobin (HGB), white blood cell (WBC), platelet (PLT), and the ratios of basophil, eosinophil, monocyte, and neutrophil were measured by Sysmex XN-9000 (Sysmex Co., Kobe, Japan). T cell, helper T cell, cytotoxic T cell, and their corresponding ratios were measured using lymphocyte detection kits (Agilent, Santa Clara, USA) by NovoCyte D2040R flow cytometry (ACEA BIO, Hangzhou, China). Cytokines, including IL-6, IL-8, and TNF-α, were measured by the Immulite 1000 (Siemens, Glyn Rhonwy, United Kingdom).

Peptide preparation for proteomic analysis

The plasma and urine samples were processed as described previously for proteomic analysis.[14] Briefly, 4 μL plasma for each sample was added to High Select Top-14 Abundant Protein Depletion Mini Spin Columns to deplete high-abundance proteins. The eluates were ultrafiltered to 50 μL using a 3K MWCO filtering unit (Thermo Fisher Scientific, San Jose, CA, USA). The concentrated samples were lysed in 50 μL buffer (8 M urea in 100 mM triethylammonium bicarbonate, TEAB) and concentrated to 50 μL. Then, the samples were reduced with 10 mM tris-(2-carboxyethyl)-phosphine (TCEP, Sigma, St Louis, MO, USA) and alkylated with 40 mM iodoacetamide (IAA, Sigma) in the dark for 30 min at 31.5°C. After the mixture was diluted with 125 μL TEAB, the plasma proteins were digested with 0.5 μg trypsin for 4 h at 32°C, followed by second digestion with 0.5 μg trypsin at the same temperature for 12 h. To stop digestion, the reaction pH was adjusted to 2∼3 by 10% trifluoroacetic acid (TFA, Sigma).

For urine peptides preparation, 500 μL urine supernatant was ultrafiltered to 100 μL using a 3K MWCO filtering unit. The concentrated sample was added to 100 μL PBS and precipitated with cold acetone to a final concentration of 80% (v/v) at -20°C overnight. The formed precipitates were harvested by centrifugation and then denatured with 25 μL 8 M urea in 100 mM TEAB. The protein solutions were reduced with 10 mM TCEP for 30 min and alkylated with 30 mM IAA for 45 min at 32°C in the dark. The mixture was then diluted with 132 μL TEAB and digested with 1 μg trypsin for 4 h at 32°C. After dilution with 30 μL TEAB, another digestion with 1 μg trypsin was performed for 12 h. The mixture was acidified with 10% TFA to stop digestion.

After desalting with SOLAμ (Thermo Fisher Scientific, San Jose, CA, USA), the plasma and urine peptides were labeled by TMTpro 16 plex reagents. The TMT peptides were eluted and separated into thirty fractions using a stepwise gradient of increasing acetonitrile at pH 10 on a DIONEX UltiMate 3000 UHPLC System (Thermo Fisher Scientific, San Jose, CA, USA) with an XBridge Peptide BEH C18 column (300 Å, 5 μm × 4.6 mm × 250 mm) (Waters, Milford, MA, USA). The thirty fractions were combined into fifteen fractions, dried in a vacuum concentrator, and then analyzed by a Q Exactive HF Hybrid Quadrupole-Orbitrap (Thermo Fisher Scientific, San Jose, CA, USA) in data-dependent acquisition (DDA) mode with the same LC-MS/MS settings as described previously.[15] For each acquisition, peptides were injected into a precolumn (3 μm, 100 Å, 20 mm×75 μm i.d.) at a flow rate of 6 μL/min for 4 min and then analyzed using a 60 min linear LC gradient from 5% to 28% buffer B (buffer A: 2% ACN, 0.1% formic acid; buffer B: 98% ACN, 0.1% formic acid) at a flow rate of 0.3 μL/min (analytical column, 1.9 μm, 120 Å, 150 mm×75 μm i.d.). For MS acquisition, the m/z range of MS1 was 350 to 1800 with a resolution of 60,000 (at 200 m/z). The AGC target was set at $3e^6$, and the maximum ion injection time (max IT) was 50 ms. The top 20 precursors were selected for the MS/MS experiment, with a resolution at 60,000 (at 200 m/z), an AGC target of $2e^5$, and a max IT of 100 ms. The isolation window of the selected precursor was 0.7 m/z. MS data were further analyzed by the Proteome Discoverer (version 2.4.1.15, Thermo Fisher Scientific) search engine against the human protein database downloaded from SwissProt.

MRM analysis in the training and test cohorts

The differentially expressed proteins of plasma and urine at D0, D14, and D42 were selected and used for a targeted MRM study. The Skyline (version 21.2) was used to generate the list of transitions for unique peptides of these selected proteins. For the experiment, a Thermo Scientific™ TSQ Altis Mass Spectrometer was operated in MS/MS mode. The digested peptides were separated at a flow rate of 300 nL/min using an analytical column (75 μm × 150 mm, 1.9 μm 120 Å C18 particles) for a total time of 45 min. Comprising 2% ACN in 0.1% formic acid as the mobile phase A and 98% ACN in 0.1% formic acid as the mobile phase B were used for the binary buffer system. All transition peaks for each target peptide were analyzed using Skyline, and all chromatograms were manually inspected to ensure the quality and accurate peak picking.

Quality control

The plasma and urine samples of the three time points in the training cohort (n= 60) were randomly distributed in 16 different batches. The pooled sample, a mixture of all peptides, was used as a control sample in each batch and labeled with TMT pro-126 to calibrate the quantitative accuracy between different batches. To ensure the quality of the proteomic data, the coefficients of the variation (CV) values of protein

abundance of the plasma and urine were first analyzed. The distribution of the urine and plasma samples in different batches was checked using PCA analysis.

Mufzz and pathway analysis

For the subcellular localization of each protein, the online UniProt database (https://www.uniprot.org/) was applied. ANOVA was applied to the proteomic data of plasma and urine collected at different time points (P value<0.05). These differentially expressed proteins were analyzed using the R package Mfuzz (version 2.48.0) and classified into eight groups. Three databases were applied for the pathway enrichment analysis, including GO biological process, KEGG pathway, and ingenuity pathway analysis (IPA).[59]

Cytokine analysis

For cytokine analysis, the IMMPORT database (Updated: July 2020) (ImmPort, 2020) was used for cytokine classification of plasma and urine protein, and 223 cytokines were classified into six types. The t-test analysis was used to determine whether the cytokines showed statistically significant differences between the high and low antibody titer groups. According to the online database immuneXpresso matching results.[60] 20 of these cytokines were associated with the functions of multiple immune cells. Finally, these proteomic data were visualized by shinyCircos (version 4.1.2).[61]

Random forest analysis

To further screen the features of plasma and urine protein for MRM analysis, the differentially expressed proteins in different time points of plasma and urine were obtained. The mass spectrometry data of these proteins were further analyzed. The spectral similarity between transition peak areas and library spectra was calculated by Skyline. Then, 43 plasma and 62 urine proteins with high-quality transition peaks were selected for MRM analysis. We subsequently built a random forest (RF) model on the training cohort using the R package Random Forest (4.6.14) as described previously and calculated the Gini index importance for each protein.[23] After optimizing the key random forest parameters, including the cutoff values for decreased mean accuracy and the number of trees, RF models were reconstructed with the selected features for plasma and urine alone, as well as the integration of the above index. Finally, all the RF models were evaluated on the test cohort to predict the ACE2-RBD-inhibiting antibody response. Antibody titers above the 50th percentile of the cohort were defined as high titers, while those below the 50th percentile were defined as low titers.

Fecal genomic DNA extraction and metagenomic sequencing and data analysis

TIANamp Stool DNA Kit (TIANGEN, Beijing, China) was used for fecal genomic DNA extraction. NanoDrop 2000C spectrophotometer (Thermo Fisher Scientific, Waltham, USA) was used for the measurement of the concentration and purity of the extracted DNA. Then the libraries were sequenced using the Illumina NovaSeq 6000 platform by Novogene (Tianjin, China). The raw data was cleaned by KneadData. Taxonomic counts were obtained by Metaphlan. The HMP Unified Metabolic Analysis Network 3.0 was applied for functional annotations. HUMAnN 3 uses MetaCyc for the pathway definitions. Maaslin 2 was applied for the analysis of differences in bacterial abundance and the Metacyc pathway. The ANOSIM test was used to calculate the significance of dissimilarity using the R Community Ecology Package vegan.

Database search

The TMT-labeled mass spectrometric data of plasma and urine were identified using Proteome Discoverer (Version 2.4.0.305, Thermo Fisher Scientific) against a manually annotated and reviewed Homo sapiens protein FASTA database (SwissProt, 27 April 2020). The enzyme was set to full-specificity trypsin with two missed cleavages. Static modifications were set to carbamidomethylation of cysteine and TMTpro of lysine residues and the N-termini of peptides. Variable modifications were set to oxidation of methionine and acetylation of the N-termini of peptides. The precursor ion mass tolerance was set to 10 ppm, and the production was set to 0.02 Da. The peptide-spectrum-match allowed a 1% target false discovery rate (FDR). The R package limma was used to analyze DEPs with a threshold of P value less than 0.05 and BH adjusted P value less than 0.05. The subcellular localization of each protein was matched on the UniProt database (https://www.uniprot.org/).

QUANTIFICATION AND STATISTICAL ANALYSIS

Normality and lognormality test (Shapiro-Wilk test) was used to test normality. If data passed the normality test, comparisons between two groups were performed using an unpaired two-tailed Student's t test. Otherwise, comparisons between two groups were performed using an unpaired two-tailed Mann-Whitney test. Pearson or Spearman correlation coefficient and two-tailed probability P value were calculated in the correlation studies.

ADDITIONAL RESOURCES

This research was registered in the Chinese Clinical Trial Registry with an ID of ChiCTR2100044919 (https://www.chictr.org.cn/showproj.html?proj=122521).